IET Energy Systems Integration

WILEY

天津大学 Tianjin University | IET The Institution of Engineering and Technology

ORIGINAL RESEARCH OPEN ACCESS

Parametric Sensitivity Analysis of a Multi-Gigawatt Offshore Multi-Energy System Using Reduced-Order Models

Nakul Narayanan K[1] | Chunjun Huang[2] | Maria Camila Castrillon Franco[2] | Jose Luis Rueda Torres[2]

[1]Department of Electrical Engineering, Government Engineering College Thrissur, Thrissur, Kerala, India | [2]Department of Electrical Sustainable Energy, Delft University of Technology, Delft, the Netherlands

Correspondence: Jose Luis Rueda Torres (J.L.RuedaTorres@tudelft.nl)

Received: 9 December 2025 | **Revised:** 24 February 2026 | **Accepted:** 13 March 2026

Keywords: eigenvalues and eigenfunctions | power system simulation | power system stability | wind power plants

ABSTRACT

When multiple grid-forming and grid-following converters operate within an offshore energy system (OES), dynamic interactions among them can lead to poorly damped oscillations and potential instability. This paper proposes a computationally efficient reduced-order state-space modelling framework for small-signal stability and parametric sensitivity analysis of large-scale OESs. The approach replaces complex full-order analytical modelling with a practical MATLAB/Simulink-based linearisation procedure, enabling tractable stability assessment of systems comprising multiple wind plants, electrolysers, HVDC links and network components. The reduced-order model preserves the dominant dynamics while significantly decreasing the number of states, thereby improving computational efficiency for eigenvalue and sensitivity analyses. Using the linearised model, the influence of key control parameters is systematically quantified to provide explicit guidance for controller tuning and damping improvement. The accuracy of the proposed model is validated through comparison with detailed electromagnetic transient (EMT) simulations in PSCAD/EMTDC, demonstrating close agreement in dynamic responses and stability characteristics.

1 | Introduction

There is an increasing focus on deploying offshore electrolyser power plants to enable large-scale green hydrogen production [1–3]. These electrolyser power plants are often connected to existing offshore wind power plants to meet their electrical power demand. Both the electrolyser plants and the wind power plants are interfaced with the offshore AC network through voltage source converters (VSCs), which are operated either in grid-following (GFL) or grid-forming mode (GFM). To support the offshore network and enable black-start capability, offshore wind power plants are typically operated in GFM [4–8], whereas electrolyser plants are operated in GFL mode. Although GFM operation has several advantages, GFM converters are prone to low-frequency resonances due to various contributing factors [9, 10]. The control design of GFM converters involves a cascaded control structure that includes an inner current loop, an outer AC voltage control loop, GFM control and DC-link voltage control [11]. The performance and tuning of these controllers are highly dependent on system parameters [12]. Although it is possible to design a single converter in GFM with sufficient stability margins [11], connecting multiple converters can make the system susceptible to low-frequency oscillations or even instability [13, 14]. The stability of GFMs when connected to a grid is widely investigated in the literature [15, 16]. Recent advancements in GFM converter stability focus on enhanced control strategies to improve performance in weak grids and under fault conditions [17], including advanced current-limiting techniques [18], virtual inertia and adaptive control. However, in all these studies, the

grid is modelled as a voltage source behind an impedance. Such a model cannot predict the interaction between multiple converters operating in different modes. When multiple converters are operated together and stability analysis is to be performed, the complete system needs to be considered as a whole.

Several methods have been explored in the literature for stability analysis of offshore energy systems, including eigenvalue analysis using state-space modelling [19], transfer-function-based analysis [20], impedance-based modelling [21], EMT time-domain simulations [22], frequency scanning [23], vector fitting (VF) techniques [24] and eigensystem realisation methods [25]. Among these, state-space analysis and impedance-based approaches are the two most widely adopted methods for assessing the stability of such interconnected converter-dominated systems [26, 27].

In impedance-based stability analysis, the system impedance can be derived analytically or extracted through time-domain simulations [28, 29]. Classical frequency-domain tools such as Nyquist or Bode plots are then employed to evaluate stability margins [30, 31]. Although these approaches are effective for assessing overall stability, they provide limited insight into the contribution of individual states and control parameters to oscillatory modes.

In contrast, state-space analysis reveals the complete dynamic behaviour of the system and enables modal and participation factor studies [32]. However, this approach requires explicit nonlinear mathematical models of all subsystems and subsequent linearisation around an operating point. For large-scale offshore energy systems composed of multiple converter-interfaced plants, constructing such unified models becomes challenging. Each plant is typically modelled in its own local *dq* reference frame, necessitating multiple frame transformations, whereas determining consistent steady-state operating points for all states is computationally intensive. Consequently, fully analytical linearisation of the entire system becomes impractical and error-prone for realistic configurations.

To address these limitations, this paper proposes a systematic reduced-order state-space modelling and analysis framework for efficient stability assessment of large-scale offshore energy systems (OESs). The main contributions of this work are threefold. First, a unified reduced-order state-space model of the complete OES, including wind power plants, electrolysers, HVDC links and network components, is developed, enabling tractable small-signal analysis of multiconverter interactions. Second, a practical MATLAB/Simulink-based linearisation procedure is adopted to automatically obtain the system Jacobian, thereby avoiding cumbersome analytical derivations for large-scale systems. Third, an eigenvalue sensitivity and participation factor analysis framework is introduced to quantitatively relate control parameters, system states and oscillatory modes, providing explicit guidance for controller tuning and damping improvement. Compared with full-order modelling and EMT simulations, the proposed approach significantly reduces computational complexity while preserving the dominant dynamics, making parametric studies and stability-oriented design feasible for realistic offshore energy systems.

The remainder of this paper is organised as follows: Section 2 describes the offshore energy system structure and control strategies. Section 3 presents the derivation of the reduced-order model. Section 4 provides the parametric sensitivity analysis and validation results. Finally, Section 5 concludes this paper and outlines future work.

2 | Description and Control of OES

The OES under consideration is illustrated in Figure 1. This configuration includes three wind power plants, two electrolyser plants and a bipolar high-voltage direct current (HVDC) link, all connected to a common AC bus. The offshore AC network is connected to the onshore AC network through the HVDC link. The wind power plants and electrolyser plants are linked to the common offshore AC bus through AC cables. Figure 2 shows the single-phase equivalent circuit diagram of a three-phase voltage source converter (VSC) typically used in the wind and electrolyser power plants. In an electrolyser plant, the DC link of the VSC is connected to the electrolyser through a DC–DC converter. For a Type-4 wind turbine plant, the permanent magnet synchronous generator is connected to the AC network through a back-to-back VSC. In the OES under consideration, the electrolyser plants are operated in GFL mode, whereas the wind power plants are operated in GFM mode. The power injected by the wind turbines and the power absorbed by the electrolyser plants at the DC link are represented using a power source P_d.

A brief review of the grid-forming and grid-following control strategies is presented below.

2.1 | Grid-Following Control of VSC

The VSC in the electrolyser plant is operated in GFL mode, with its primary control objective being the regulation of the DC voltage to a specified reference. The DC–DC converter interfaced with the DC link operates under a constant-power control mode. When the control bandwidth of the power controller is sufficiently high, the electrolyser, along with the DC–DC converter, can be represented as a constant-power load from the perspective of the DC-link dynamics. The converter control structure is shown in Figure 3. The inner current controller, $C_i(s)$, and the DC voltage controller, $F_{dc}(s)$, are designed to ensure sufficient stability margins for the system [33]. The PLL controller, $C_{pll}(s)$, is designed for a specified bandwidth, as described in Ref. [34].

2.2 | Grid-Forming Control of VSC

The VSC interfaced with the AC network of the wind power plant operates in GFM mode. The most commonly used GFM control methods include power synchronisation control, droop

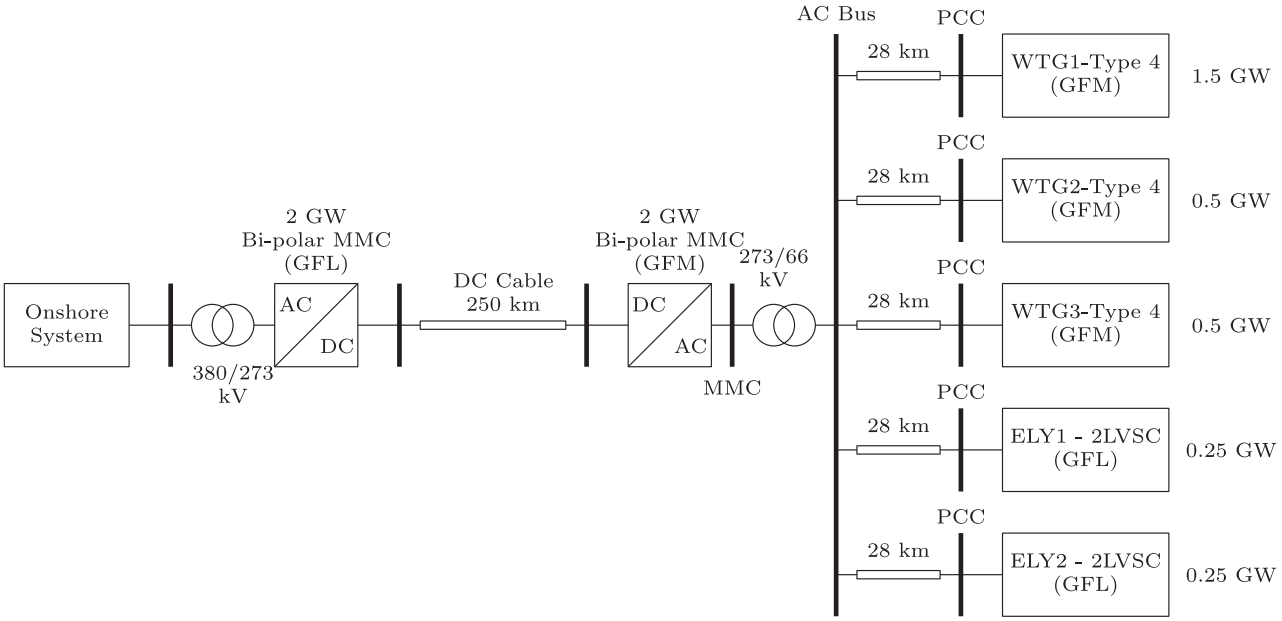

FIGURE 1 | Simplified single-line diagram of offshore energy system under consideration. ELY, electrolyser plant; WTG, wind turbine generator plant.

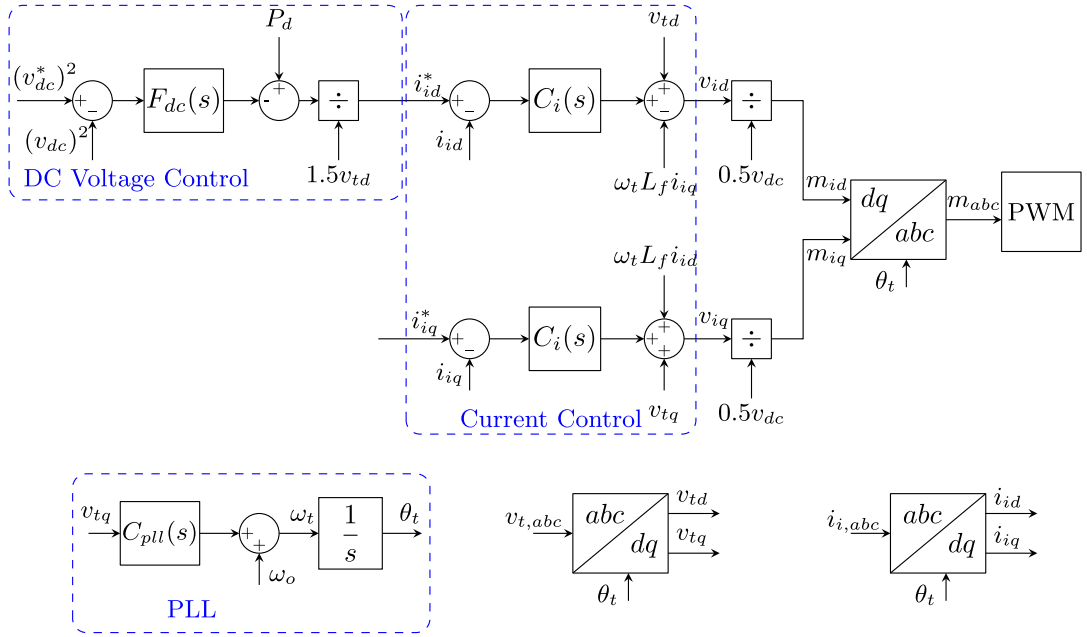

FIGURE 2 | Single-phase equivalent circuit of VSC (X_t transformer impedance).

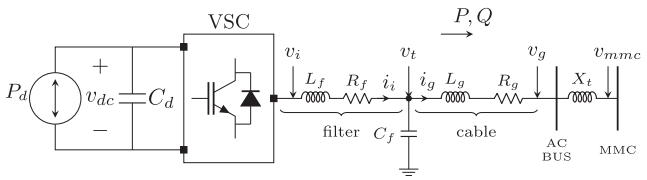

FIGURE 3 | Control block diagram of the GFL converter.

control and virtual synchronous machine control [35]. In this system, the widely used droop-control-based GFM strategy is implemented, enabling the converter to emulate the dynamic behaviour of a synchronous generator for the regulation of both active and reactive power. This is achieved by applying droop characteristics to the voltage vector magnitude ($\hat{V}$) and frequency (ω_t) at the point of common coupling (PCC). The active and reactive powers are controlled based on the following control law [35]:

$$\begin{aligned} \omega_t &= \omega_o + (P_o - P)\, m_P, \\ \hat{V} &= \hat{V}^* + (Q_o - Q)\, m_Q, \end{aligned} \tag{1}$$

where ω_o and $\hat{V}^*$ are the reference frequency and voltage magnitude at the PCC, respectively; P_o and Q_o are the reference active and reactive powers, respectively; and m_P and m_Q are the

active and reactive power droop coefficients, respectively. The control structure of the converter with droop-based GFM control in the dq reference frame is shown in Figure 4. The reference active power P_o is derived from the DC voltage controller. The DC voltage controller, $F_{dc}(s)$, can be implemented as a simple proportional gain K_d when appropriate feedforward terms are included [11]. The inner current controller, $C_i(s)$, and the DC voltage controller, $F_{dc}(s)$, are designed to ensure sufficient stability margins for the system [11, 33]. Because of the limited interaction between the dynamics of the wind turbine generator and the AC network, the wind turbine can be modelled as a power source [36].

The offshore HVDC converter is also operated in GFM mode, with the objective of maintaining a constant voltage and frequency at the MMC bus, as shown in Figure 1. The control structure of the offshore HVDC converter is similar to that of the grid-side converter of the wind turbine. The only difference is that the angle θ is generated based on the reference frequency, whereas the d- and q-axis voltage references are kept constant.

2.3 | Dynamic Performance of the OES

The dynamic performance of the OES is validated through detailed time-domain simulations in PSCAD, with all power plants operating at their nominal capacity. At time $t = 3$ s, the power input of a 1.5-GW wind turbine generator is changed from 1.0 p.u. to 0.75 p.u. Figure 5 illustrates the system's dynamic behaviour in response to a step change in the power. From the simulation results, the following observations can be made:

- The power output changes smoothly from 1.0 p.u. to 0.75 p.u. without any oscillations, reflecting a stable system behaviour.
- The actual current tracks the reference current closely, demonstrating accurate current regulation.

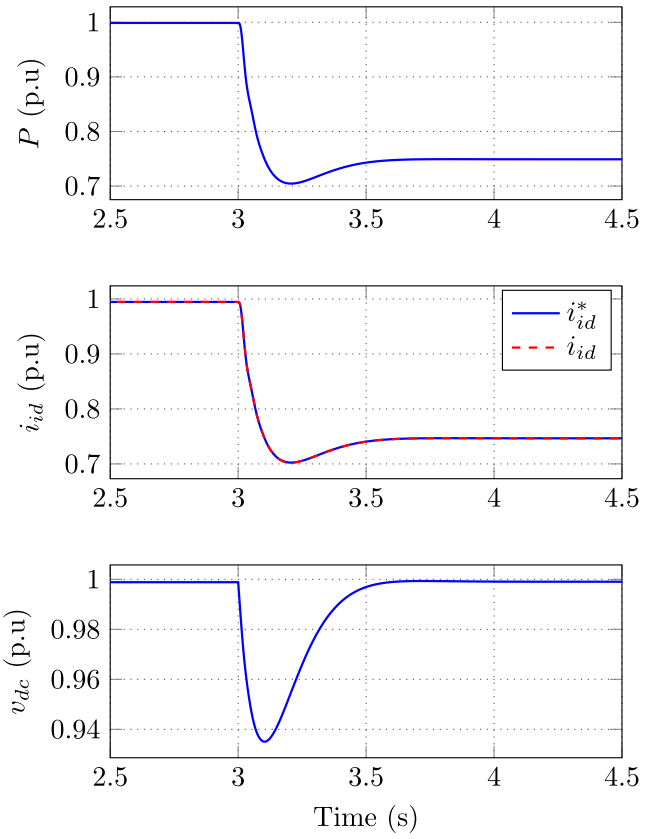

FIGURE 5 | Response of active power output, filter d-axis current and DC-link voltage for a step change in active power reference.

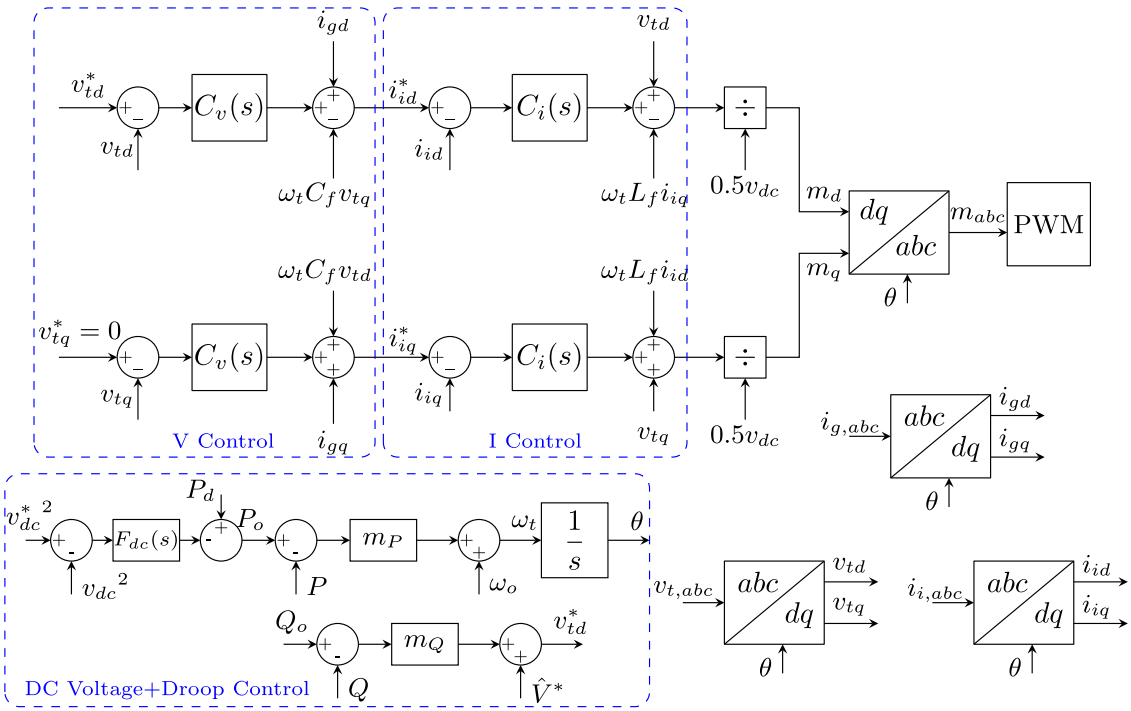

FIGURE 4 | Control block diagram of the droop-based GFM control.

- The DC-link voltage experiences a brief drop during the adjustment but subsequently stabilises back to 1.0 p.u.

Based on the above observations, it can be concluded that when system parameters are accurately known, the controls can be well designed. However, in practical scenarios, some system parameters may be partially unknown or may deviate from their nominal values. In the following section, a mathematical model is developed to analyse the impact of parameter variations on system stability and performance.

3 | Reduced-Order Small-Signal Modelling of OES

The dynamics and stability of the system can be analysed by developing a state-space model of the system. This model can be derived using either a full-order or a reduced-order modelling approach. In the full-order state-space modelling approach, the complete mathematical model of the system, including the controllers, is derived. This includes the phase-locked loop (PLL), the inner current control loop, the AC voltage control loops, the GFM control loop and the outer DC voltage control loop. The control loops operate with varying bandwidths, with some designed for fast (high-bandwidth) responses and others for slower (low-bandwidth) dynamics.

In the reduced-order modelling approach, the dynamics of the faster loops are neglected. Because the typical underdamped oscillations in the OES occur in the subsynchronous frequency range [37], this modelling approach is appropriate. In both GFM and GFL control schemes, the inner current loop is the fastest, typically designed with a bandwidth around one tenth of the switching frequency. Therefore, in the reduced-order model, the dynamics of the inner current loops are neglected. The reduced-order models for the various power plants within the OES are presented below.

3.1 | Reduced-Order Model of GFL

The electrolyser plant, along with its control system as shown in Figures 2 and 3, respectively, consists of a total of 11 states when modelled in the *dq* frame. These include two states for the filter inductor (L_f) currents, two states for the grid inductor (L_g) currents, two states for the filter capacitor (C_f) voltages, one state for the DC-link capacitor, two states for the inner current control and two states for the PLL.

As discussed earlier, the inner current loop exhibits significantly faster dynamics and can therefore be neglected in the reduced-order model. This implies that the converter is assumed to perfectly track the current reference. As a result, the states associated with the inner current control and the filter inductor currents are eliminated, reducing the total number of states from 11 to seven. When the DC voltage controller bandwidth is much higher than the oscillation frequencies in the OES, the DC side can be represented using a DC voltage source [27]. By neglecting the states associated with the inner current control, filter inductor currents and DC voltage dynamics, the total number of states in the system is further reduced to six. The reduced-order model of the plant and the controller is illustrated in Figure 6.

3.2 | Reduced-Order Model of GFM Converter

The wind power plant, along with its control system as shown in Figures 2 and 7, respectively, when modelled in the *dq* frame, consists of a total of 12 states. These include two states for the filter inductor (L_f) currents, two for the grid inductor (L_g) currents and two for the filter capacitor (C_f) voltages. The model also includes one state for the DC-link capacitor, two for the inner current control loops, two for the outer voltage control loops and one for the droop control.

As noted in the previous sections, the inner current loop dynamics are typically designed to be much faster, allowing the states associated with the inner current control and the filter inductor currents to be neglected. However, compared to the GFL converter, the DC-link dynamics in the GFM converter cannot be neglected, as they are part of the lowest-bandwidth control loop. In the GFM control structure, the control hierarchy typically starts with the fast inner current control loop, followed by the slower AC voltage control loop. This AC voltage control loop is then cascaded with the GFM control loop, which operates with an even lower bandwidth. As a result, the overall control structure leads to slow DC-link dynamics that must be retained in the reduced-order model for accurate representation. Therefore, in the reduced-order model, the total number of states is reduced from 12 to eight. The resulting model and the control structure of the GFM converter are shown in Figure 7.

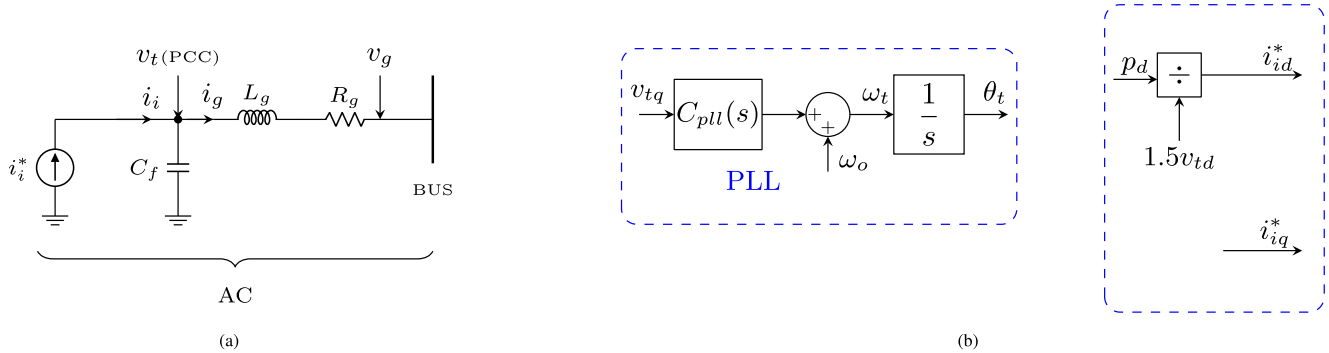

FIGURE 6 | (a) Single-phase equivalent circuit of reduced-order model of GFL converter; (b) reduced-order model of GFL converter control.

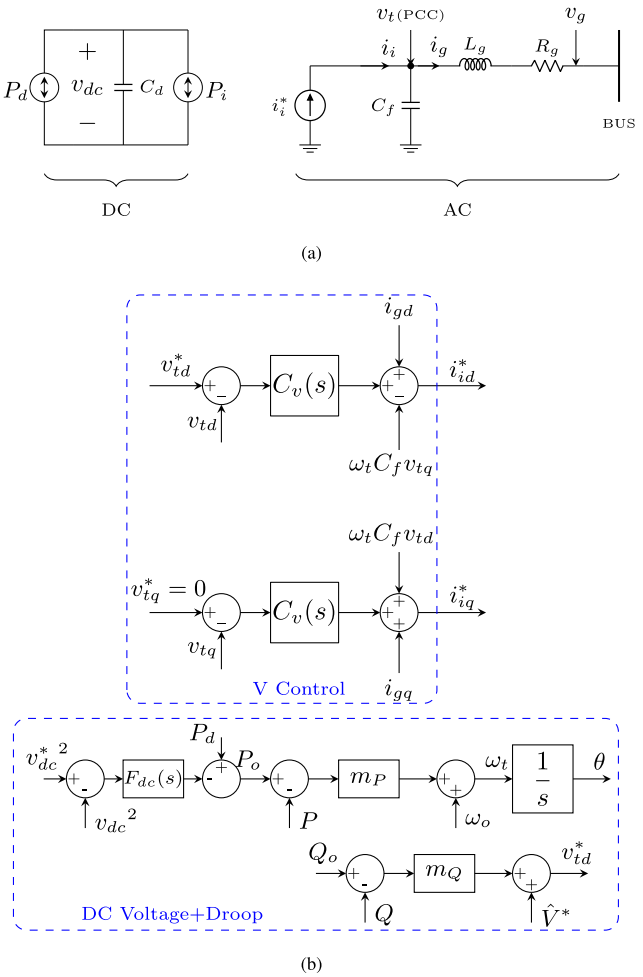

FIGURE 7 | (a) Single-phase equivalent circuit of reduced-order model of GFM; (b) reduced-order control structure of GFM control.

3.3 | Reduced-Order Model of OES

The total order of the complete offshore energy system model, including all wind plants, electrolysers, HVDC links and network components, is 62 states for the full-order model. After applying the proposed model reduction, the order is reduced to 40 states while preserving the dominant dynamic modes relevant to stability analysis.

The reduced-order dynamics of the entire OES consist of the dynamics of the GFM and GFL converters, as well as the dynamics of the interconnecting cables. Although these dynamics are still interconnected, building a fully analytical model for large-scale systems remains infeasible. Instead, a more practical approach involves constructing a reduced-order OES in MATLAB Simulink. In this approach, the individual models of the electrolyser and wind power plants are built in their local dq reference frames. The currents and voltages from the local dq frames need to be transferred to a global reference frame to model the dynamics of the interconnection cables. In Simulink, this can be done more easily than in an analytical model. This approach avoids the complexity of analytical frame transformations and provides the system operating point directly from simulation, eliminating the need to solve the full nonlinear equations analytically. The reduced-order model remains nonlinear and can subsequently be linearised for further analysis, enabling practical and scalable modelling of large-scale systems.

The linearisation is performed by simulating the OES in MATLAB/Simulink to establish steady-state operating conditions. MATLAB's built-in **linearise** function is then used to generate a linearised state-space model at the operating point. This linearised model of the OES can be expressed as follows:

$$\begin{aligned} \Delta\dot{\mathbf{X}} &= \mathbf{A}\Delta\mathbf{X} + \mathbf{B}\Delta\mathbf{U} \\ \Delta\mathbf{Y} &= \mathbf{C}\Delta\mathbf{X} + \mathbf{D}\Delta\mathbf{U} \end{aligned} \tag{2}$$

where $\mathbf{X}$ and $\mathbf{U}$ represent the state and input vectors, respectively, whereas $\mathbf{A}$, $\mathbf{B}$, $\mathbf{C}$ and $\mathbf{D}$ denote the state-space matrices of the entire OES. The **linearise** function provides the state-space matrices along with the system's eigenvalues and the corresponding right and left eigenvectors. These outputs can be further utilised to identify oscillatory modes within the system and to calculate participation factors and eigenvalue sensitivities with respect to parameter variations [32].

Before proceeding with the sensitivity analysis, the accuracy of the linearised reduced-order model is first validated by comparing its step–response behaviour with that of the nonlinear time-domain model. A comparison is carried out between detailed EMT simulations in PSCAD and the reduced-order state-space model implemented in MATLAB/Simulink. Several disturbances under different operating points are applied, and the corresponding responses are compared to verify the validity of the proposed model. The nominal design values of the DC voltage controller gain and the droop gain are 5 p.u. and $m_P = 3.7$ p.u., respectively.

In Figure 8a, a 0.05-p.u. step change in active power is applied to the 1.5-GW wind turbine generator at $t = 5$ s while operating at 1 p.u. In Figure 8b, a 0.025-p.u. step change in the DC voltage reference is introduced at the same operating point. In Figure 8c, a 0.025-p.u. DC voltage reference step is applied when the plant operates at 0.5 p.u. Finally, Figure 8d shows the response to a 0.1-p.u. active power step change. The close match between the PSCAD and reduced-order model responses confirms that the dominant dynamics are accurately captured by the proposed linearised model.

Moreover, from the simulation results shown in Figure 8a, the oscillation frequency of the d-axis current injected into the network is measured to be approximately 5.01 Hz. The system eigenvalues obtained from the linearised state matrix $\mathbf{A}$ are plotted in Figure 9. The dominant complex-conjugate pair, λ_i and $\overline{\lambda}_i$, is located at $-7.295 \pm j\,31.45$. These eigenvalues predict an oscillation frequency of approximately 5 Hz (31.45 rad/s), which closely matches the frequency observed in the time-domain simulations. Similar step disturbances can be applied at different operating points in both models, and the resulting responses can be compared to further validate the effectiveness and accuracy of the proposed linearised reduced-order model.

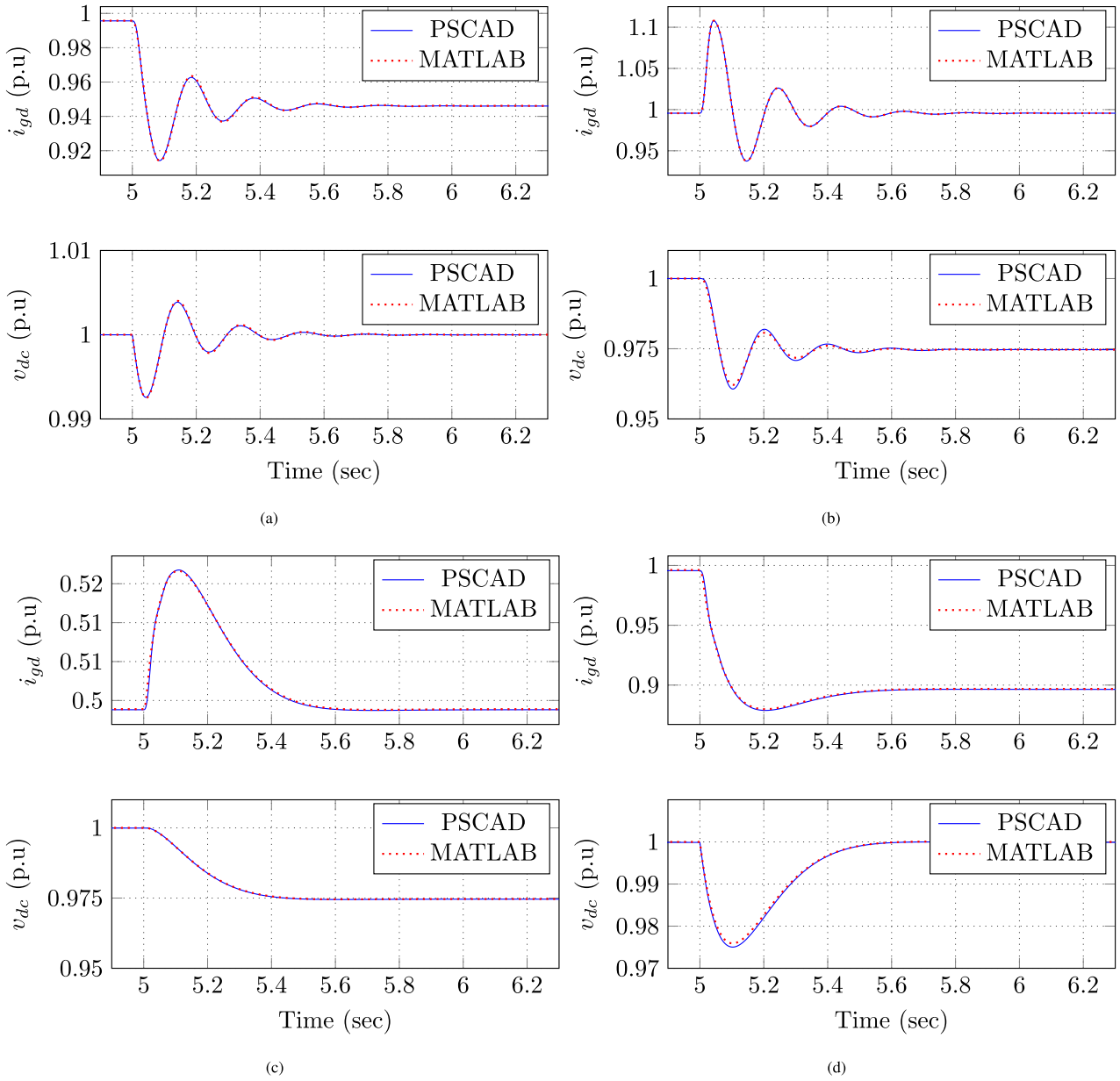

FIGURE 8 | Comparison of PSCAD and MATLAB (reduced-order model) simulations: (a) for a 0.05-p.u. step disturbance in active power under droop control; (b) for a 0.025-p.u. step change in DC voltage reference at 1 p.u. active power; (c) for a 0.025-p.u. step change in DC voltage reference at 0.5 p.u. active power; (d) for a 0.1-p.u. step disturbance in active power under droop control.

4 | Sensitivity Analysis

A sensitivity analysis is performed on the OES to evaluate the impact of parameter variations on system stability and performance using the linearised small-signal model developed in the previous section. The control design for each power plant in the OES relies on system parameters such as grid impedance and operating conditions. However, discrepancies may exist between the actual system parameter values and those assumed during the design process. Such discrepancies may lead to undesired oscillations or even system instability. Sensitivity analysis helps in developing a control design that is more robust to these uncertainties [12]. In this section, the reduced-order model of the OES is employed to carry out the sensitivity analysis.

The sensitivity analysis of the OES is performed by varying selected system parameters and tracking the loci of the dominant eigenvalues. Initially, the OES is simulated in MATLAB/Simulink to determine the steady-state operating points corresponding to each parameter sweep. For each operating condition, the model is then linearised and the eigenvalues are computed. These eigenvalues are subsequently used to evaluate system stability and dynamic behaviour. The overall procedure is summarised in the flow chart shown in Figure 10.

Further insight into the relationship between the system state variables and the oscillatory modes (eigenvalues) can be obtained by performing a participation factor analysis of the state matrix. The participation factor P_{ki} quantifies the extent to

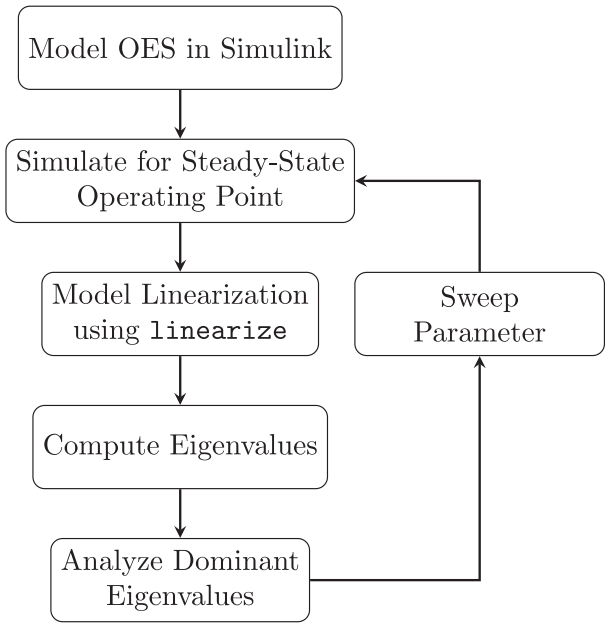

FIGURE 9 | Dominant eigenvalues from the reduced-order model under droop control (dashed lines: grid of constant damping factors).

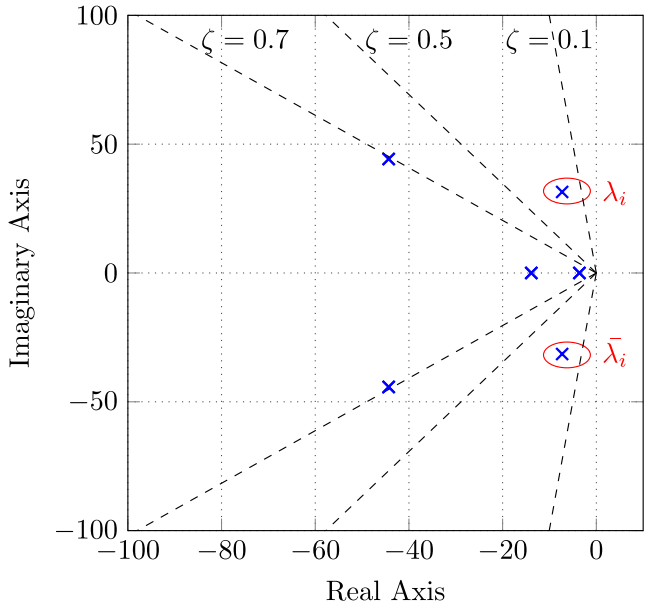

FIGURE 10 | Flow chart of the sensitivity analysis process.

which the i^{th} state participates in the k^{th} mode. The normalised participation factor is given by the following equation:

$$P_{ki} = \frac{|\phi_{ik}\,\psi_{ki}|}{\sum_{j=1}^{n} |\phi_{jk}\,\psi_{kj}|} \tag{3}$$

where ϕ_{ik} and ψ_{ki} denote the i^{th} elements of the right and left eigenvectors associated with the k^{th} eigenvalue, respectively, and n is the total number of state variables in the system.

In the OES, the droop coefficient m_P and the DC voltage controller gain K_d of the wind turbine generator are designed based on the knowledge of system parameters. Sensitivity analysis is therefore carried out to quantify the impact of these parameters on system stability. These parameters are specifically selected because a higher droop gain improves the transient response of the OES, whereas a larger DC voltage control gain increases the bandwidth of the DC voltage controller [27].

Figure 11 shows the movement of a pair of eigenvalues as the DC voltage controller gain K_d of wind turbine generator 1 is varied from 0.5 p.u. to 50 p.u. From Figure 1, the base value of K_d can be inferred as the ratio of the square of the DC voltage base value to the power rating. As observed from the plot, increasing K_d causes the eigenvalues to move towards the right-half plane, resulting in reduced damping. This behaviour leads to oscillations in the OES. A further increase in K_d shifts the eigenvalues into the right-half plane, rendering the system unstable. This instability is further confirmed by the participation factor analysis.

The analysis is performed for $K_d = 50$, where a pair of eigenvalues, $11.75 \pm j\,98.63$, lies in the right-half plane (RHP), indicating unstable oscillatory behaviour. The results show that the states x_{15} and x_{18} have the highest participation in these modes, corresponding to the droop angle and the DC-link voltage of wind turbine 1, respectively. This demonstrates that the DC-link voltage dynamics and their associated controller have a dominant influence on the unstable mode. Consequently, an excessively high DC-link voltage controller gain has a destabilising effect, pushing the system into oscillatory instability.

In addition, a time-domain simulation is carried out to verify the instability predicted by the eigenvalue analysis when the DC voltage controller gain is increased. The gain K_d is changed from 20 to 30 at $t = 5$ s, and the results are shown in Figure 12. The eigenvalue analysis indicates that the system is stable for $K_d = 20$, whereas the dominant poles move to the right-half plane for $K_d = 30$, indicating instability. The time-domain response corroborates this prediction, showing growing oscillations after the gain increase.

A similar analysis is performed by varying the droop gain m_P. Figure 13 shows the movement of a pair of eigenvalues as m_P is increased from 30 p.u. to 200 p.u. As observed from the plot, increasing m_P causes the eigenvalues to shift towards the right-half plane with reduced damping, resulting in oscillations in the OES. Further increases in m_P push the eigenvalues deeper into the right-half plane, leading to system instability. The participation factor analysis further substantiates this instability.

The analysis is performed for $m_P = 200$, where a pair of eigenvalues, $53.31 \pm j\,364.87$, lies in the right-half plane (RHP), indicating unstable oscillatory behaviour. The results show that the state x_{15} exhibits the highest participation in this unstable mode, corresponding to the droop angle of wind turbine 1. This finding indicates that an excessively high droop gain has a destabilising effect, driving the system into oscillatory instability.

Although the analysis in this study focuses on two key parameters of the grid-forming converter, the same procedure can be readily extended to other system parameters, such as PLL bandwidth, transmission cable length, converter power rating and active/

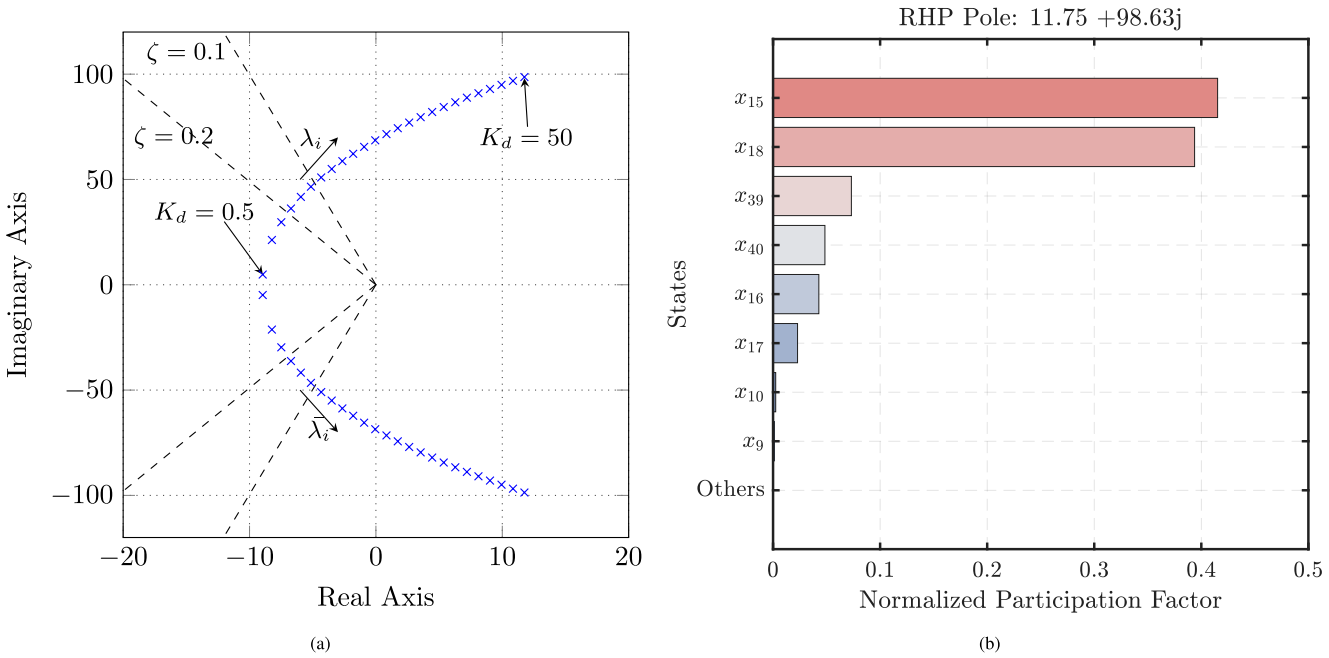

(a) (b)

FIGURE 11 | (a) Eigenvalue locus with change in DC voltage controller gain K_d (dashed lines: grid of constant damping factors). (b) Normalised participation factor.

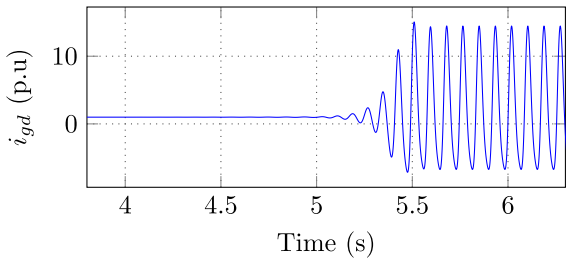

FIGURE 12 | Time-domain response when K_d is varied from 20 to 30.

reactive power set-points. The participation factor analysis presented in the previous section has already identified the states that predominantly contribute to the critical oscillatory modes. Building on these results, a parametric sensitivity analysis is subsequently carried out to quantitatively evaluate how variations in the control gains associated with those dominant states influence the corresponding eigenvalues and system damping.

The sensitivity of the ith eigenvalue with respect to a parameter p is computed as follows:

$$\frac{\partial \lambda_i}{\partial p} = \frac{\psi_i^{\mathrm{T}} \left(\frac{\partial A}{\partial p} \right) \phi_i}{\psi_i^{\mathrm{T}} \phi_i}, \tag{4}$$

where ϕ_i and ψ_i denote the right and left eigenvectors associated with λ_i, respectively.

Using this formulation, a sensitivity analysis is performed for the dominant oscillatory mode identified in Figure 9. The sensitivity of this mode with respect to the DC voltage controller gain K_d is then computed, and the results are summarised in Table 1.

The results in Table 1 indicate that the identified low-frequency oscillatory mode (≈5 Hz) exhibits a high positive real-part sensitivity with respect to K_d. Specifically, $\partial \mathrm{Re}(\lambda_i)/\partial K_d = 4.4115$ implies that increasing the DC voltage controller gain shifts the pole towards the right-half plane, thereby reducing damping. Consequently, even moderate increases in K_d may destabilise the system. This observation confirms that the DC voltage controller gain strongly influences the dominant dynamics and must be carefully tuned to maintain adequate stability margins.

From the participation factor analysis, the dominant mode is primarily associated with the droop-angle and DC-link voltage states. Combined with the high eigenvalue sensitivity to K_d, this result indicates that the DC voltage controller directly excites these states and reduces damping.

5 | Conclusion

This paper developed a reduced-order modelling framework for the parametric sensitivity analysis of offshore energy system stability. Reduced-order models of the electrolyser and wind power plants were derived and linearised using built-in MATLAB/Simulink functions. The accuracy of the linearised models was validated through comparisons with EMT time-domain simulations.

The resulting linearised models were then employed to evaluate the sensitivity of key system parameters. The analysis demonstrated that the DC voltage controller gain and the active power droop gain have a significant influence on the dominant eigenvalues and that improper tuning of these parameters can drive the system towards instability. Participation factor analysis of the critical modes was also conducted to identify the most influential state variables, providing deeper insight into the

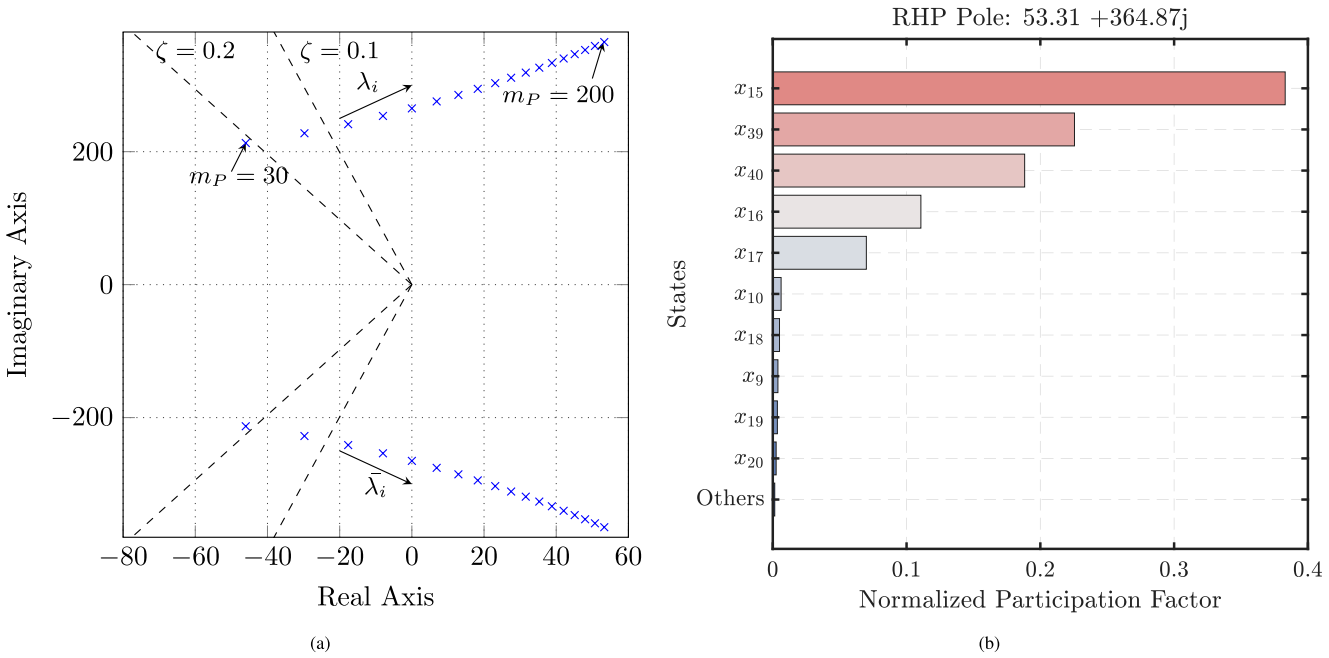

FIGURE 13 | (a) Eigenvalue locus with change in active power droop gain m_P (dashed lines: grid of constant damping factors). (b) Normalised participation factor.

TABLE 1 | Sensitivity of dominant oscillatory mode with respect to K_d.

Mode (λ_i)	Frequency (Hz)	Damping ratio ζ	$\partial \mathrm{Re}(\lambda_i)/\partial K_d$
$-7.295 \pm j\,31.45$	5.01	0.226	4.4115

sources of oscillatory behaviour. In addition, eigenvalue sensitivity analysis quantified how strongly the dominant eigenvalues vary with respect to the controller gains.

The proposed methodology offers a computationally efficient tool for stability assessment and can be readily extended to other system variables. From a practical perspective, the obtained sensitivity information provides clear guidance for controller design and re-tuning, enabling the appropriate selection of gains to ensure adequate damping and stable operation of large-scale offshore energy systems.

Acknowledgements

The research work shown in this paper has received funding from TenneT TSO BV within the research project on 'Adaptive identification and mitigation of variable oscillatory phenomena in weakening networks - FORBES' and 'Adaptive fast active power control for stabilisation of multiconverter dynamics in offshore electrical energy-hydrogen hubs - FUTURE SYSTEM'. It reflects only the authors' views, and the aforesaid organisation is not responsible for any use that may be made of the paper's content.

Conflicts of Interest

The authors declare no conflicts of interest.

Data Availability Statement

No data are available.

References

1. S. Ramakrishnan, M. Delpisheh, C. Convery, D. Niblett, M. Vinothkannan, and M. Mamlouk, "Offshore Green Hydrogen Production From Wind Energy: Critical Review and Perspective," *Renewable and Sustainable Energy Reviews* 195 (2024): 114320, https://doi.org/10.1016/j.rser.2024.114320.

2. G. Liu and P. Mancarella, "Integrated Techno-Economic Assessment of Large-Scale Green Hydrogen Production," in *Proceedings of the 2021 IEEE Madrid PowerTech* (2021), 1–6, https://doi.org/10.1109/PowerTech46648.2021.9494961.

3. A. Flah, H. Kraiem, M. Jayachandran, et al., "Advancing Sustainable Energy Transition Through Green Hydrogen Valleys," *IEEE Access* 13 (2025): 31442–31471, https://doi.org/10.1109/ACCESS.2025.3542554.

4. R. Rosso, X. Wang, M. Liserre, X. Lu, and S. Engelken, "Grid-Forming Converters: Control Approaches, Grid-Synchronization, and Future Trends—–A Review," *IEEE Open Journal of Industry Applications* 2 (2021): 93–109, https://doi.org/10.1109/OJIA.2021.3074028.

5. R. Aljarrah, B. B. Fawaz, Q. Salem, M. Karimi, H. Marzooghi, and R. Azizipanah-Abarghooee, "Issues and Challenges of Grid-Following Converters Interfacing Renewable Energy Sources in Low Inertia Systems: A Review," *IEEE Access* 12 (2024): 5534–5561, https://doi.org/10.1109/ACCESS.2024.3349630.

6. X. Fu, J. Sun, M. Huang, et al., "Large-Signal Stability of Grid-Forming and Grid-Following Controls in Voltage Source Converter: A Comparative Study," *IEEE Transactions on Power Electronics* 36, no. 7 (2021): 7832–7840, https://doi.org/10.1109/TPEL.2020.3047480.

7. X. Lyu and D. Groß, "Grid Forming Fast Frequency Response for PMSG-Based Wind Turbines," *IEEE Transactions on Sustainable Energy* 15, no. 1 (2024): 23–38, https://doi.org/10.1109/TSTE.2023.3263858.

8. R. Alves, A. Egea-Àlvarez, and T. Knuppel, "Grid Forming and Grid Following Comparison for an Offshore Wind Farm Connected via a HVAC Cable," in *Proceedings of the 21st Wind & Solar Integration Workshop (WIW 2022)* (2022), 9–16, https://doi.org/10.1049/icp.2022.2729.

9. Z. Zeng, P. M. Gajare, D. Divan, and M. Saeedifard, "Impact of DC Voltage Reference on Subsynchronous Dynamics in Grid-Forming Inverters," *IEEE Transactions on Power Electronics* 40, no. 7 (2025): 8934–8938, https://doi.org/10.1109/TPEL.2025.3548013.

10. L. Zhao, Z. Jin, and X. Wang, "Analysis and Damping of Low-Frequency Oscillation for DC-Link Voltage-Synchronized VSCs," *IEEE Transactions on Power Electronics* 38, no. 7 (2023): 8177–8189, https://doi.org/10.1109/TPEL.2023.3263577.

11. F. Zhao, T. Zhu, L. Harnefors, et al., "Closed-Form Solutions for Grid-Forming Converters: A Design-Oriented Study," *IEEE Open Journal of Power Electronics* 5 (2024): 186–200, https://doi.org/10.1109/OJPEL.2024.3357128.

12. S. D'Arco, J. A. Suul, and O. B. Fosso, "Automatic Tuning of Cascaded Controllers for Power Converters Using Eigenvalue Parametric Sensitivities," *IEEE Transactions on Industry Applications* 51, no. 2 (2015): 1743–1753, https://doi.org/10.1109/TIA.2014.2354732.

13. T. Gebremedhin, Y. Chen, L. Xu, and D. Chen, "Interactions and Stability Analysis of Grid-Forming and Grid-Following Converters in Close Proximity: An Impedance-Based Approach," *IET Conference Proceedings* 2024, no. 32 (2024): 263–269, https://doi.org/10.1049/icp.2024.4588.

14. X. Wang and F. Blaabjerg, "Harmonic Stability in Power Electronic-Based Power Systems: Concept, Modeling, and Analysis," *IEEE Transactions on Smart Grid* 10, no. 3 (2019): 2858–2870, https://doi.org/10.1109/TSG.2018.2812712.

15. F. Zhao, T. Zhu, Z. Li, and X. Wang, "Low-Frequency Resonances in Grid-Forming Converters: Causes and Damping Control," *IEEE Transactions on Power Electronics* 39, no. 11 (2024): 14430–14447, https://doi.org/10.1109/TPEL.2024.3424296.

16. X. Gao, D. Zhou, A. Anvari-Moghaddam, and F. Blaabjerg, "Stability Analysis of Grid-Following and Grid-Forming Converters Based on State-Space Modelling," *IEEE Transactions on Industry Applications* 60, no. 3 (2024): 4910–4920, https://doi.org/10.1109/TIA.2024.3353158.

17. Z. Sun, Z. He, N. Liu, R. Zhang, B. Wang, and G. Cai, "Enhanced Transient Stability Strategy for Grid-Forming Converter Based on Current Limiting," *CSEE Journal of Power and Energy Systems* 11, no. 3 (2025): 960–971, https://doi.org/10.17775/CSEEJPES.2024.08620.

18. N. Baeckeland, D. Chatterjee, M. Lu, B. Johnson, and G. S. Seo, "Overcurrent Limiting in Grid-Forming Inverters: A Comprehensive Review and Discussion," *IEEE Transactions on Power Electronics* 39, no. 11 (2024): 14493–14517, https://doi.org/10.1109/TPEL.2024.3430316.

19. Y. Xu, M. Zhang, L. Fan, and Z. Miao, "Small-Signal Stability Analysis of Type-4 Wind in Series-Compensated Networks," *IEEE Transactions on Energy Conversion* 35, no. 1 (2020): 529–538, https://doi.org/10.1109/TEC.2019.2943578.

20. L. Sainz, L. Monjo, M. Cheah-Mane, and J. Liang, "Assessment of Subsynchronous Oscillations in AC Grid-Connected VSC Systems With Type-4 Wind Turbines," *IET Renewable Power Generation* 13, no. 16 (2019): 3088–3096, https://doi.org/10.1049/iet-rpg.2019.0291.

21. M. Amin and M. Molinas, "Understanding the Origin of Oscillatory Phenomena Observed Between Wind Farms and HVdc Systems," *IEEE Journal of Emerging and Selected Topics in Power Electronics* 5, no. 1 (2017): 378–392, https://doi.org/10.1109/JESTPE.2016.2620378.

22. Y. Li, L. Fan, and Z. Miao, "Replicating Real-World Wind Farm SSR Events," *IEEE Transactions on Power Delivery* 35, no. 1 (2020): 339–348, https://doi.org/10.1109/TPWRD.2019.2931838.

23. A. Rygg and M. Molinas, "Apparent Impedance Analysis: A Small-Signal Method for Stability Analysis of Power Electronic-Based Systems," *IEEE Journal of Emerging and Selected Topics in Power Electronics* 5, no. 4 (2017): 1474–1486, https://doi.org/10.1109/JESTPE.2017.2729596.

24. M. K. Bakhshizadeh, F. Blaabjerg, J. Hjerrild, Ł. Kocewiak, and C. L. Bak, "Improving the Impedance-Based Stability Criterion by Using the Vector Fitting Method," *IEEE Transactions on Energy Conversion* 33, no. 4 (2018): 1739–1747, https://doi.org/10.1109/TEC.2018.2849347.

25. L. Fan and Z. Miao, "Time-Domain Measurement-Based *DQ*-Frame Admittance Model Identification for Inverter-Based Resources," *IEEE Transactions on Power Systems* 36, no. 3 (2021): 2211–2221, https://doi.org/10.1109/TPWRS.2020.3040360.

26. M. Amin and M. Molinas, "Small-Signal Stability Assessment of Power Electronics Based Power Systems: A Discussion of Impedance- and Eigenvalue-Based Methods," *IEEE Transactions on Industry Applications* 53, no. 5 (2017): 5014–5030, https://doi.org/10.1109/TIA.2017.2712692.

27. N. Pogaku, M. Prodanovic, and T. C. Green, "Modeling, Analysis and Testing of Autonomous Operation of an Inverter-Based Microgrid," *IEEE Transactions on Power Electronics* 22, no. 2 (2007): 613–625, https://doi.org/10.1109/TPEL.2006.890003.

28. S. Shah, P. Koralewicz, V. Gevorgian, H. Liu, and J. Fu, "Impedance Methods for Analyzing Stability Impacts of Inverter-Based Resources: Stability Analysis Tools for Modern Power Systems," *IEEE Electrification Magazine* 9, no. 1 (2021): 53–65, https://doi.org/10.1109/MELE.2020.3047166.

29. R. H. Ramakrishna, Z. Miao, L. Fan, and S. Shah, "DQ Admittance Extraction for Inverter-Based Resources," in *2023 IEEE Power & Energy Society General Meeting (PESGM)* (2023), 1–5, https://doi.org/10.1109/PESGM52003.2023.10253247.

30. L. Fan and Z. Miao, "Admittance-Based Stability Analysis: Bode Plots, Nyquist Diagrams or Eigenvalue Analysis?," *IEEE Transactions on Power Systems* 35, no. 4 (2020): 3312–3315, https://doi.org/10.1109/TPWRS.2020.2996014.

31. J. Sun, "Impedance-Based Stability Criterion for Grid-Connected Inverters," *IEEE Transactions on Power Electronics* 26, no. 11 (2011): 3075–3078, https://doi.org/10.1109/TPEL.2011.2136439.

32. P. Kundur, *Power System Stability and Control* (McGraw-Hill, 1994).

33. A. Yazdani and R. Iravani, *Voltage-Sourced Converters in Power Systems: Modeling, Control, and Applications* (John Wiley & Sons, 2010).

34. S. K. Chung, "Phase-Locked Loop for Grid-Connected Three-Phase Power Conversion Systems," *IEE Proceedings - Electric Power Applications* 147, no. 3 (2000): 213–219, https://doi.org/10.1049/ip-epa:20000328.

35. D. Pan, X. Wang, F. Liu, and R. Shi, "Transient Stability of Voltage-Source Converters With Grid-Forming Control: A Design-Oriented Study," *IEEE Journal of Emerging and Selected Topics in Power Electronics* 8, no. 2 (2020): 1019–1033, https://doi.org/10.1109/JESTPE.2019.2946310.

36. S. Liu, R. G. Cirstea, H. Wu, T. Bosma, and X. Wang, "Comparative Evaluation of Converter Control Impact on Torsional Dynamics of Type-IV Grid-Forming Wind Turbines," *IEEE Transactions on Sustainable Energy* 15, no. 4 (2024): 2803–2814, https://doi.org/10.1109/TSTE.2024.3444474.

37. B. Shao, S. Zhao, Y. Yang, B. Gao, and F. Blaabjerg, "Sub-Synchronous Oscillation Characteristics and Analysis of Direct-Drive Wind Farms With VSC-HVDC Systems," *IEEE Transactions on Sustainable Energy* 12, no. 2 (2021): 1127–1140, https://doi.org/10.1109/TSTE.2020.3035203.